Title

Targeting NOX4 alleviates sepsis-induced acute lung injury via attenuation of redox-sensitive activation of CaMKII/ERK1/2/MLCK and endothelial cell barrier dysfunction

Authors

Jiang, Jinyao
Huang, Kai
Xu, Shiqing
et al.

Publication Date

2020-09-01

DOI

10.1016/j.redox.2020.101638

Peer reviewed

Redox Biology 36 (2020) 101638

Contents lists available at ScienceDirect

Redox Biology

journal homepage: www.elsevier.com/locate/redox

Research Paper

Targeting NOX4 alleviates sepsis-induced acute lung injury via attenuation of redox-sensitive activation of CaMKII/ERK1/2/MLCK and endothelial cell barrier dysfunction

Jinyao Jiang [a], Kai Huang [b], Shiqing Xu [a], Joe G.N. Garcia [c], Chen Wang [a,d,**], Hua Cai [b,*]

[a] Department of Pulmonary and Critical Care Medicine, China-Japan Friendship Hospital, Capital Medical University, Beijing, China
[b] Division of Molecular Medicine, Department of Anesthesiology, Division of Cardiology, Department of Medicine, David Geffen School of Medicine, University of California Los Angeles, Los Angeles, CA, USA
[c] Department of Medicine, University of Arizona, Tucson, AZ, USA
[d] Institute of Respiratory Medicine, Chinese Academy of Medical Sciences and Peking Union Medical College, Beijing, China

ARTICLE INFO

Keywords:
Acute lung injury (ALI)
Acute respiratory distress syndrome (ARDS)
NADPH oxidase (NOX)
NOX1
NOX2
NOX4
p22phox
p47phox
Reactive oxygen species (ROS)
Endothelial cell (EC)
Endothelial barrier dysfunction
Endothelial permeability
Tight junction
ZO-1
Occludin

ABSTRACT

Increased pulmonary vascular permeability due to endothelial cell (EC) barrier dysfunction is a major pathological feature of acute respiratory distress syndrome/acute lung injury (ARDS/ALI), which is a devastating critical illness with high incidence and excessive mortality. Activation of NADPH oxidase (NOX) induces EC dysfunction via production of reactive oxygen species (ROS). However, the role(s) of NOX isoform(s), and their downstream signaling events, in the development of ARDS/ALI have remained unclear. Cecal Ligation Puncture (CLP) was used to induce preclinical septic ALI in wild-type mice and mice deficient in NOX2 or p47phox, or mice transfected of control siRNA, NOX1 or NOX4 siRNA in vivo. The survival rate of the CLP group at 24 h (26.6%, control siRNA treated) was substantially improved by NOX4 knockdown (52.9%). Mice lacking NOX2 or p47phox, however, had worse outcomes after CLP (survival rates at 0% and 8.3% respectively), whereas NOX1-silenced mice had similar survival rate (30%). NOX4 knockdown attenuated lung ROS production in septic mice, whereas NOX1 knockdown, NOX2 knockout, or p47phox knockout in mice had no effects. In addition, NOX4 knockdown attenuated redox-sensitive activation of the CaMKII/ERK1/2/MLCK pathway, and restored expression of EC tight junction proteins ZO-1 and Occludin to maintain EC barrier integrity. Correspondingly, NOX4 knockdown in cultured human lung microvascular ECs also reduced LPS-induced ROS production, CaMKII/ERK1/2/MLCK activation and EC barrier dysfunction. Scavenging superoxide *in vitro* and *in vivo* with TEMPO, or inhibiting CaMKII activation with KN93, had similar effects as NOX4 knockdown in preserving EC barrier dysfunction. In summary, we have identified a novel, selective and causal role of NOX4 (versus other NOX isoforms) in inducing lung EC barrier dysfunction and injury/mortality in a preclinical CLP-induced septic model, which involves redox-sensitive activation of CaMKII/ERK1/2/MLCK pathway. Targeting NOX4 may therefore prove to an innovative therapeutic option that is markedly effective in treating ALI/ARDS.

1. Introduction

Acute respiratory distress syndrome (ARDS) is a devastating clinical condition characterized by refractory hypoxemia, respiratory distress, and non-cardiogenic pulmonary edema [1]. Despite significant advances in our understanding and management of ARDS, treatment options for ARDS remain limited to enable substantial improvement in survival; and the mortality rate is over 40% in the United States [2,3]. A key pathological feature of ARDS is the disruption of lung endothelial barrier integrity [4–7]. The endothelium is a monolayer that lines the luminal surface of the vasculature and provides a semipermeable barrier between circulating blood and underlying tissues. In ARDS, a disrupted endothelial barrier due to exuberant inflammatory responses leads to increased pulmonary vascular permeability to circulating fluids,

* Corresponding author. Department of Anesthesiology, Department of Medicine, David Geffen School of Medicine, University of California Los Angeles, USA.
** Corresponding author. Department of Pulmonary and Critical Care Medicine, China-Japan Friendship Hospital, Institute of Respiratory Medicine, Chinese Academy of Medical Sciences and Peking Union Medical College, China.
E-mail addresses: wangchen66366@163.com (C. Wang), hcai@mednet.ucla.edu (H. Cai).

https://doi.org/10.1016/j.redox.2020.101638
Received 25 May 2020; Received in revised form 1 July 2020; Accepted 3 July 2020
Available online 13 July 2020

macromolecules, and leukocytes, resulting in alveolar flooding and neutrophil influx [8], contributing to the high mortality of ARDS. Accordingly, targeting endothelial barrier integrity may represent a valuable strategy for development of novel therapeutics for ARDS.

Oxidative stress has been shown to play a major role in the progression of ARDS [9–13]. Low levels of ROS serve as vital signaling molecules under physiological conditions [14]. During ARDS however, the production of ROS is increased to result in leakage of fluids, and penetration of neutrophils and lymphocytes from pulmonary blood vessels, as well as exacerbation of pulmonary inflammation and development of edema [9]. NADPH oxidase (NOX) family of proteins represent the primary enzymatic sources of ROS during cardiovascular pathogenesis, which provoke oxidative inactivation of NO and consequent uncoupling of eNOS, leading to sustained oxidative stress [15]. Four of the NOX isoforms, NOX1, NOX2, NOX4 and NOX5 are expressed in endothelial cells [15], while NOX5 is absent in rodents and cannot be studied in mice [16]. Additionally, as the only membrane-bound subunit, p22phox is necessary for the stability and activation of NOX1, NOX2 and NOX4 [15,17]. Phosphorylation and membrane translocation of the cytosolic subunit p47phox is required for assembly and activation of NOX1 and NOX2 [15,18,19]. However, roles and mechanisms of NOX isoforms in ARDS/ALI remain unclear.

Ca^{2+}/calmodulin-dependent protein kinase II (CaMKII) is a ubiquitous kinase that is activated by an elevation in intracellular Ca^{2+} [20]. CaMKII is also redox-sensitive and can be activated by increased levels of ROS [21,22]. ROS-dependent phosphorylation increases CaMKII sensitivity to calcium [23]. Endothelial barrier dysfunction associated with ARDS has been shown to be at least in part attributed to CaMKII activation [21,24]. Activation of CaMKII leads to hyperphosphorylation of the downstream ERK1/2/MLCK pathway [21,24], which in turn induces contraction of the peri-junctional actomyosin ring to cause assembly and disassembly of the actin cytoskeleton and disruption of intercellular junctions [25–27]. Adjacent endothelial cells are connected by intercellular junctions, including tight junctions, adherens junctions, and gap junctions [28,29]. Tight junctions and adherens junctions are formed by transmembrane proteins which construct a zig-zag mosaic along the interendothelial cell border, serving as a blood vessel barrier, while gap junctions are responsible for intercellular communication [30]. In endothelial cells, tight junctions consist of Occludin and claudins which interact with intracellular zonula occludins (ZOs, including ZO-1, ZO-2, and ZO-3) [27], and function to seal the intercellular space to maintain vascular homeostasis [27]. Among tight junctions, Occludin is a primary transmembrane protein, while ZO-1 provides a direct linkage between the actin cytoskeleton and the transmembrane proteins. Since the cytoplasmic junction proteins directly interact with the cytoskeleton, the contraction of the actomyosin ring thereby provides force for disruption of intercellular junctions, therefore inducing endothelial barrier dysfunction.

In the present study, Cecal Ligation Puncture (CLP) was used to induce septic ALI in wild-type (WT) mice and mice deficient in NOX2 or p47phox, or mice transfected with control siRNA, NOX1 or NOX4 siRNAs in vivo. We aimed to define the potential specific roles and mechanisms of NOX isoforms and their regulatory subunits in CLP-induced lung EC barrier dysfunction and disease outcome during ALI. We found that inhibition of NOX4, rather than reductions in activities of NOX1, NOX2, or p47phox, significantly improved survival and markedly attenuated vascular leakage and lung edema. NOX4 knockdown alleviated CLP-induced oxidative stress, down-regulated redox-sensitive CaMKII/ERK1/2/MLCK phosphorylation, and preserved expression of endothelial cell tight junction proteins ZO-1 and Occudin, therefore protecting against pulmonary hyperpermeability. Correspondingly, NOX4 knockdown in cultured human lung microvascular endothelial cells also reduced LPS-induced ROS production, CaMKII/ERK1/2/MLCK activation and barrier dysfunction. Scavenging superoxide *in vitro* and *in vivo* with TEMPO, or inhibiting CaMKII activation with KN93, preserved EC barrier integrity, which is consistent with the effects of NOX4 knockdown. These data demonstrate a novel, selective and causal role of NOX4 in inducing EC barrier dysfunction to result in lung injury/mortality in a preclinical model of CLP-induced sepsis. Targeting NOX4 may therefore represent a novel therapeutic strategy for the treatment of ALI/ARDS.

2. Methods

2.1. Animal studies

Eight to ten weeks old male C57BL/6 mice were obtained from Charles River Laboratory (Beijing, China). NOX2-null and p47phox-null founder mice were originally purchased from Jackson Laboratory (Bar Harbor, Maine, strain 002365 and 004742, respectively). Mice were bred and maintained under specific pathogen–free conditions. All mice were randomly assigned to experimental animal groups. The use of animals and experimental procedures were approved by the Institutional Animal Care and Usage Committee at the China-Japan Friendship Hospital.

2.2. CLP model and tissue collection

Mice were fasted, with only free access to water for 12 h prior to surgery. Subsequently, mice were anesthetized with 5% isoflurane and maintained at 2 L/min air flow using Gas Anesthesia Systems (Shanghai Yuyan Instruments Co.Ltd., Shanghai, China). Skin was disinfected and a 1 cm incision was made in the middle of the abdomen, allowing the cecum to be exposed; and a 4-0 braided silk suture was passed through the midpoint between the colon root and cecum terminal to ligate the cecum. A 21-gauge needle was inserted into the ligated cecum and a small drop of the intestinal content was squeezed out to induce infection. Finally, the cecum was repositioned and the incision was closed. For the sham group, the abdomen was opened, and then the incision was closed. Except for survival curve analyses, mice were harvested 16 h later; 50 μl heparin was injected into the right ventricle and 1 ml Krebs/HEPES buffer (KHB: 99 mmol/L NaCl; 4.7 mmol/L KCl; 1.2 mmol/L MgSO4; 1.0 mmol/L KH2PO4; 2.5 mmol/L CaCl2; 25 mmol/L NaHCO3; 5.6 mmol/L D-glucose; 20 mmol/L NaHEPES) was then injected into right ventricle to flush pulmonary vessels. The lungs were rapidly removed, rinsed in ice-cold KHB and cleaned of connective tissue on ice, and injected of KHB via pulmonary artery. The left lobe of the lung was fixed in 10% formalin for subsequent histological analyses. The right upper lobe of the lung was embedded in optimum cutting temperature compound (OCT), immediately frozen at -20 °C and sectioned at 5 μm for dihydroethidium (DHE) fluorescent imaging determination of ROS production, or immunofluorescent staining of ZO-1 and Occludin. Other lung lobes were frozen at -80 °C and homogenized for Western blotting analyses.

2.3. RNA interference of NOX1 and NOX4 in vivo

The control small interfering RNA (siRNA) (Cat#: D-001210-01-50) and the siRNA specifically designed to silence NOX1 or NOX4 expression in vivo were obtained from Dharmacon (Chicago, IL, USA). The sequences used to target NOX1 and NOX4 were as the followings as we previously published [31]: NOX1: GCUGGUGGCUGGUGACGAAUU. NOX4: CAUGCUGCUGCUGUUGCAUGUUUCA. For in vivo RNA interference, siRNA was prepared in cationic liposome-based Invivofectamine 3.0 Reagent (Cat#: IVF3005, Invitrogen, Grand Island, NY, USA). In brief, 50 μl siRNA at 2.4 mg/ml in DNase/RNase-free water was mixed with 50 μl complexation buffer, and then mixed with 100 μl Invivofectamine 3.0 Reagent. The diluted siRNA solution was vortexed immediately and incubated at 50 °C for 30 min. The transfection mixture was then diluted 6-fold with 1 ml PBS, and then in vivo delivered into mice through tail vein injection at final concentration of 1 mg/kg body weight. Mice were injected once every 48 h and CLP model was started

24 h after the first injection.

2.4. Survival analysis

For survival curve analysis, mice were observed for survival status every 30 min 12 h after CLP surgery, to record the natural death time after initiation of the CLP. The survival curve was analyzed and presented as Kaplan-Meier plot [31,32] using Prism software.

2.5. Lung histology and lung injury score

Lung tissues fixed in 10% formalin were dehydrated, paraffin embedded, sectioned, and stained with hematoxylin and eosin (H&E) for histological analyses. Severity of lung injury was scored using a semi-quantitative scoring system as described previously [33]. Inflammation (red arrows), edema (blue arrows), hemorrhage (black arrows), and alveolar septal thickening (green arrows) were each scored on a 0- to 4-point scale: Inflammation was assessed by counting the total number of inflammatory cells/×100 field; 5–7 random fields were counted per slide. Edema and hemorrhage were categorized as the followings: absent (score = 0), mild (<10% alveoli involved; score = 1), moderate (10–30% alveoli involved; score = 2), severe (10–30% alveoli involved; score = 3), or very severe (>50% alveoli involved; score = 4). Alveolar septal thickening was measured and categorized as the followings: photographs taken at 400x magnification were used to measure the vertical distance at the thickest part of the alveolar septum, divided by 400 to get the thickness of alveolar septum into the following categories; absent (thickness of alveolar septum<15 μm; score = 0), mild (thickness of alveolar septum in 15–30 μm; score = 1), moderate (thickness of alveolar septum in 30–45 μm; score = 2), severe (thickness of alveolar septum in 45–60 μm; score = 3), or very severe (thickness of alveolar septum>60 μm; score = 4). Inflammation, edema, hemorrhage, and alveolar septal thickening scores for each group were averaged, and the final score represents the overall assessment from all four injury parameters.

2.6. Lung Evans Blue index

To measure endothelial permeability in the lung, Evans Blue dye extravasation assay was performed as previously described [34]. In brief, Evans Blue was injected into mice via tail vein and allowed to circulate for 30 min. At harvest, intravascular Evans Blue was washed by KHB perfusion from the right ventricle for 2 min. Mouse lungs were then excised, weighed, homogenized in 1 ml KHB, and placed in 2 ml formamide at 60°C overnight. Evans Blue concentration in supernatants was quantified spectrophotometrically at 620 nm.

2.7. Lung wet-to-dry weight ratio

The lung wet-to-dry weight ratio was used as an index of pulmonary edema that is reflective of severity of increased endothelial permeability and lung injury. Lung tissues were weighed immediately after removal (wet weight), and then placed into a 60°C oven for 48 h. The dried lung was re-weighed again (dry weight). The ratio of the lung weight before and after drying (wet/dry) was calculated.

2.8. Western blotting

Lung tissues were powderized in liquid nitrogen before lysis with lysis buffer (50 mmol/l Tris pH 7.4, 2 mmol/l EDTA, 1 mmol/l EGTA) containing 1% Triton X-100, 0.1% sodium dodecyl sulphate (SDS), 50 mmol/l NaF, 10 mmol/l $Na_4P_2O_7$, 1 mmol/l Na_3VO_4, 1 mmol/l dithiothreitol (DTT), 1 mmol/l phenylmethylfonyl-sulfonyl fluoride (PMSF) and 10 μl/ml protease inhibitor cocktail (Sigma-Aldrich) [34]. Forty microgram proteins were separated in 10% SDS-PAGE and transferred to polyvinylidene fluoride membranes (Millipore Corp, billerica, MA, USA). After 1 h blocking in PBST (PBS with 0.1% Tween-20) containing 5% (w/v) non-fat dry milk, the membranes were incubated with primary antibodies for NOX1 (1:200, Cat#: SC-5821, Santa Cruz Biotechnology Inc, Santa Cruz, CA), NOX2 (1:200, Cat#: SC-130543, Santa Cruz Biotechnology Inc, Santa Cruz, CA), NOX4 (1:500, Cat#: NB110-58849, Novus Biologicals, Littleton, CO, USA), ZO-1 (1:1,000, Cat#: 61–7300, Invitrogen, Carlsbad, CA, USA), Occludin (1:1,000, Cat#: 33–1500, Invitrogen, Carlsbad, CA, USA), p-CaMKII (1:200, Cat#: SC-32289, Santa Cruz Biotechnology Inc, Santa Cruz, CA), CaMKII (1:200, Cat#: SC-5306, Santa Cruz Biotechnology Inc, Santa Cruz, CA), p-ERK1/2 (1:1000, Cat#: 4370, Cell Signaling, Danvers, MA, USA), ERK1/2 (1:1000, Cat#: 4695, Cell Signaling Technology, Danvers, MA, USA), p-MLCK (1:1000, Cat#: 44-1085G, Invitrogen, Carlsbad, CA, USA), MLCK (1:1000, Cat#: PA5-15176, Invitrogen, Carlsbad, CA, USA) or β-actin (1:3,000, Cat#: ab8227, Abcam, Cambridge, UK) at 4°C overnight, and subsequently with peroxidase-conjugated secondary antibodies for 1 h at room temperature. Proteins were then visualized using electrochemiluminescence reagents (Cat#: WBKLS0100, Millipore Corp, Billerica, MA, USA) and quantified using the NIH Image J software.

2.9. DHE determination of ROS production

Freshly prepared lung OCT sections were incubated with freshly prepared dihydroethidium (DHE) (2 μmol/L) (Cat#: D7008, Sigma-Aldrich, St. Louis, MO, USA) in the dark for 30 min at room temperature. After washing three times with KHB, a cover slip was placed on the section, and fluorescent images were captured using a Nikon A1R Confocal Microscope (Tokyo, Japan).

2.10. Immunohistochemical analyses

Formalin-fixed, paraffin-embedded tissue sections were dewaxed, hydrated, heated for 10 min, and treated with 3% H_2O_2 for 30 min, and then incubated with normal goat serum for 60 min. Sections were incubated with rabbit anti-ZO-1 antibody (1:200) or mouse anti-Occludin antibody (1:100) at 4°C overnight. After washing, the sections were incubated with biotin-labeled goat anti-rabbit/mouse secondary antibody (Cat#: ZLI9019, Zhongshan Company, Beijing) for 60 min at 37°C. The color reaction was developed by diaminobenzidine reagent (Cat#: ZLI9019, Zhongshan Company, Beijing). Slides were counterstained with hematoxylin, and a cover slip was placed on slides before imaging with an Olympus BX53 microscope (Olympus, Japan).

2.11. Immunofluorescent analyses

Freshly prepared lung OCT sections were incubated with 0.2% Triton X-100 in PBS for 15 min followed by 5% bovine serum albumin for 30 min at room temperature. The slides were then incubated with rabbit anti-ZO-1 antibody (1:200) and mouse anti-Occludin antibody (1:100) respectively at 4°C overnight. After washing, the slides were incubated with FITC-labeled goat anti-rabbit or goat anti-mouse secondary antibody respectively for 60 min at room temperature. Slides were counterstained with DAPI, cover-slipped, and fluorescent images captured using a Nikon A1R Confocal Microscope (Tokyo, Japan).

2.12. Cell culture and NOX4 siRNA transfection in vitro

Primary human pulmonary microvascular endothelial cells (HPMECs) were purchased from Lonza (Walkersville, MD, USA) and cultured in full media (EGM-2 media from LONZA with 5% fetal bovine serum and growth factors) in a humidified incubator at 37°C with 5% CO_2. Cells were seeded into six-well plates, grown to 95% confluence, and transfected with human NOX4 siRNA (Cat#: SC-41586, Santa Cruz) or negative control siRNA (Cat#: SC-37007, Santa Cruz) using the transfection reagent Lipofectamine RNAiMAX (Cat#: 13778030, Invitrogen) following the manufacturer's instructions. In brief, 10 μl siRNA

at 20 μmol/L in DNase/RNase-free water and 10 μl Lipofectamine RNAiMAX reagent were mixed with 200 μl Opti-MEM medium (Invitrogen, Carlsbad, CA, USA); and the mixture incubated at room temperature for 5 min. The siRNA transfection reagent mixture was then used to treat cells (final concentration for siRNA: 40 nmol/L). Western blotting was used to examine efficacies of NOX4 siRNA transfection on silencing NOX4 protein expression in HPMECs.

2.13. Measurement of transendothelial electrical resistance

Transendothelial electrical resistance (TEER) measurements were performed by electric cell substrate impedance sensing system (ECIS) (Applied Biophysics, Troy, NY, USA). Human pulmonary microvascular endothelial cells (HPMECs) were grown as a confluent monolayer in ECIS array plates coated with 0.1% gelatin. Cells were then transfected with NOX4 siRNA (final concentration at 40 nmol/L) for 24 h as described above, and then treated with 1 μg/ml LPS (Cat# L3024, Sigma-Millipore, St Louis, MO, USA). TEER values were obtained every 3 min for 8 h after LPS treatment as an automatically recorded resistance (TEER = $R_{TEER} \times M_{area}$ (cm^2), R_{TEER} represents the monolayer cell resistance). The relative TEER values were calculated by dividing actual TEER values at each time point by the initial TEER values.

2.14. Statistical analysis

All statistical analyses were performed using the Prism software. All data are presented as Mean±SEM. Student's *t*-test was used to compare means between two groups, while ANOVA was used to compare multiple groups with a Bonferroni's post hoc test. The significance value is set at p less than 0.05.

3. Results

3.1. NOX4 knockdown markedly improves survival and attenuates acute lung injury in CLP-induced septic mice

To examine potential differential roles of NOX isoforms in controlling survival outcomes in CLP-induced septic mice, survival curves were analyzed by calculating numbers of survived mice in different groups up to 24 h post CLP. Control siRNA transfection did not affect the survival of CLP-induced mice. In CLP-induced control siRNA treated and WT mice, the survival rates were at 26.6% and 28.6% respectively at 24 h (vs. 100% in sham-operated mice) (Fig. 1A); *In vivo* silencing of NOX4 with RNAi substantially improved survival rate in septic mice (52.9% vs. 26.6% for NOX4 siRNA vs. control siRNA transfected mice), whereas mice lacking NOX2 or p47phox had worse outcomes after CLP, with survival rates at 0% and 8.3% respectively at 24 h. In addition, NOX1 knockdown in mice had no effects on survival rate (30% vs. 26.6% for NOX1 siRNA vs. control siRNA transfected mice) (Fig. 1A).

Alveolar flooding and neutrophil influx due to increased pulmonary vascular permeability contribute to high mortality in ALI/ARDS. To examine the potential roles of NOX isoforms in pulmonary vascular hyperpermeability, we examined pathophysiological phenotypes of septic mouse lungs in CLP-stimulated WT mice/control siRNA transfected mice, and mice deficient in NOX isoforms. At 16 h after CLP, control siRNA transfected/WT mice showed a substantial increase in lung vascular leakiness characterized by edema, alveolar and interstitial hemorrhage, alveolar septal thickening, as well as inflammatory cell infiltration, which were completely abrogated in NOX4 knockdown mice (but not in NOX1 knockdown, NOX2 knockout, or p47phox knockout mice) (Fig. 1B).

The lung wet-to-dry ratio in CLP-induced control siRNA transfected/WT mice was increased dramatically compared to the sham group (Fig. 1C), which was accompanied by an increase in Evans Blue leakage (Fig. 1D). RNAi knockdown of NOX4 substantially reduced lung wet-to-dry ratio, and prevented Evans Blue leakage in CLP-induced ALI mice. Whereas, NOX1 knockdown, NOX2 knockout, or p47phox knockout had no effects on the lung wet-to-dry ratio or the Evans Blue leakage in CLP-induced ALI mice (Fig. 1C–D). These results indicate that pulmonary hyperpermeability during sepsis induced ALI is mediated by activation of NOX4 rather than other NOX isoforms.

3.2. NOX4 knockdown reduces superoxide production and p22phox expression in CLP-induced septic mice

NOX-derived ROS induce endothelial dysfunction to contribute to cardiovascular pathogenesis [15]. We assessed ROS production using DHE fluorescent imaging in CLP-treated control siRNA transfected/WT mice, and mice deficient in specific NOX isoforms. The stained tissue sections showed a strong red fluorescence produced from DHE oxidization by superoxide under conditions of sepsis. NOX4 knockdown markedly attenuated increased DHE fluorescent signals in response to sepsis. However, NOX1 knockdown, NOX2 knockout, or p47phox knockout had no effects on DHE fluorescent intensities under septic condition (Fig. 2A).

We further examined protein expression of NOX1, NOX2 and NOX4 in CLP mice. Of note, NOX4 protein expression was rapidly and persistently unregulated by CLP, starting at 1 h and lasted through 4 h (Fig. 2B). In contrast, NOX1 upregulation was delayed and transient, occurring at 2 h post CLP and lasted for less than 2 h, and the magnitude of upregulation was lower than NOX4 (2.4-fold vs. 3.9-fold for NOX1 upregulation vs. NOX4 upregulation at 2 h). Of note, NOX2 was upregulated at 2 h post CLP, and the magnitude of upregulation was also lower than NOX4 (2.2-fold vs. 3.9-fold for NOX2 upregulation vs. NOX4 upregulation at 2 h).

Each NOX isoform is composed of one catalytic subunit and other regulatory subunits, except for NOX5, which is not expressed in rodents. As the only membrane bound subunit that is required for activation of NOX isoforms, p22phox contributes to stability and activation of NOX1, NOX2, NOX3 (only in fetal tissue and the inner ear), and NOX4 [15]. Therefore, we further examined protein expression of p22phox in CLP-induced septic mice. Results indicate that p22phox protein expression was significantly increased as early as 1 h after CLP (Fig. 2B), coinciding with the time point of initial upregulation of NOX4.

As shown in Fig. 2C–F, protein expression of NOX1, NOX2, NOX4 or p47phox in the lung tissues was effectively attenuated by specific knockout or RNAi-based knockdown. *In vivo* RNAi attenuated NOX1 or NOX4 expression while NOX2 and p47phox knockout mice showed no expression of target proteins (Fig. 2C–F). We also examined the effects of NOX1, NOX2, NOX4 or p47phox knockdown/knockout on expression of other NOX isoforms to examine potential compensatory responses. Results show that NOX1 knockdown had no effect on the expression of NOX2 and NOX4, nor on the expression of p22phox (Fig. 2C), while NOX4 knockdown significantly reduced protein abundance of p22phox although it had no effects on the protein levels of NOX1 and NOX2 (Fig. 2E). The abrogated p22phox expression may additionally contribute to the beneficial effects of NOX4 knockdown. However, NOX2 knockout led to increased expression of NOX4, and p22phox, and this response may in part explain the exaggerated injury in NOX2 knockout mice (Fig. 2D). Likewise, p47phox knockout mice also had upregulated p22phox expression (Fig. 2F).

3.3. NOX4 knockdown prevents CLP-induced pulmonary hyperpermeability via CaMKII/ERK1/2/MLCK pathway inactivation

CaM Kinase II is redox-sensitive and a known mediator of endothelial barrier dysfunction in sepsis-induced ALI by activation of ERK1/2/MLCK pathway [21]. Therefore, we next examined roles of CaMKII activation and its downstream effectors in NOX4-mediated pulmonary hyperpermeability. Interestingly, CaMKII Thr-286 phosphorylation was significantly increased 1 h and 2 h after CLP (Fig. 3A), which is consistent with rapid upregulation in NOX4 protein expression (Fig. 2B).

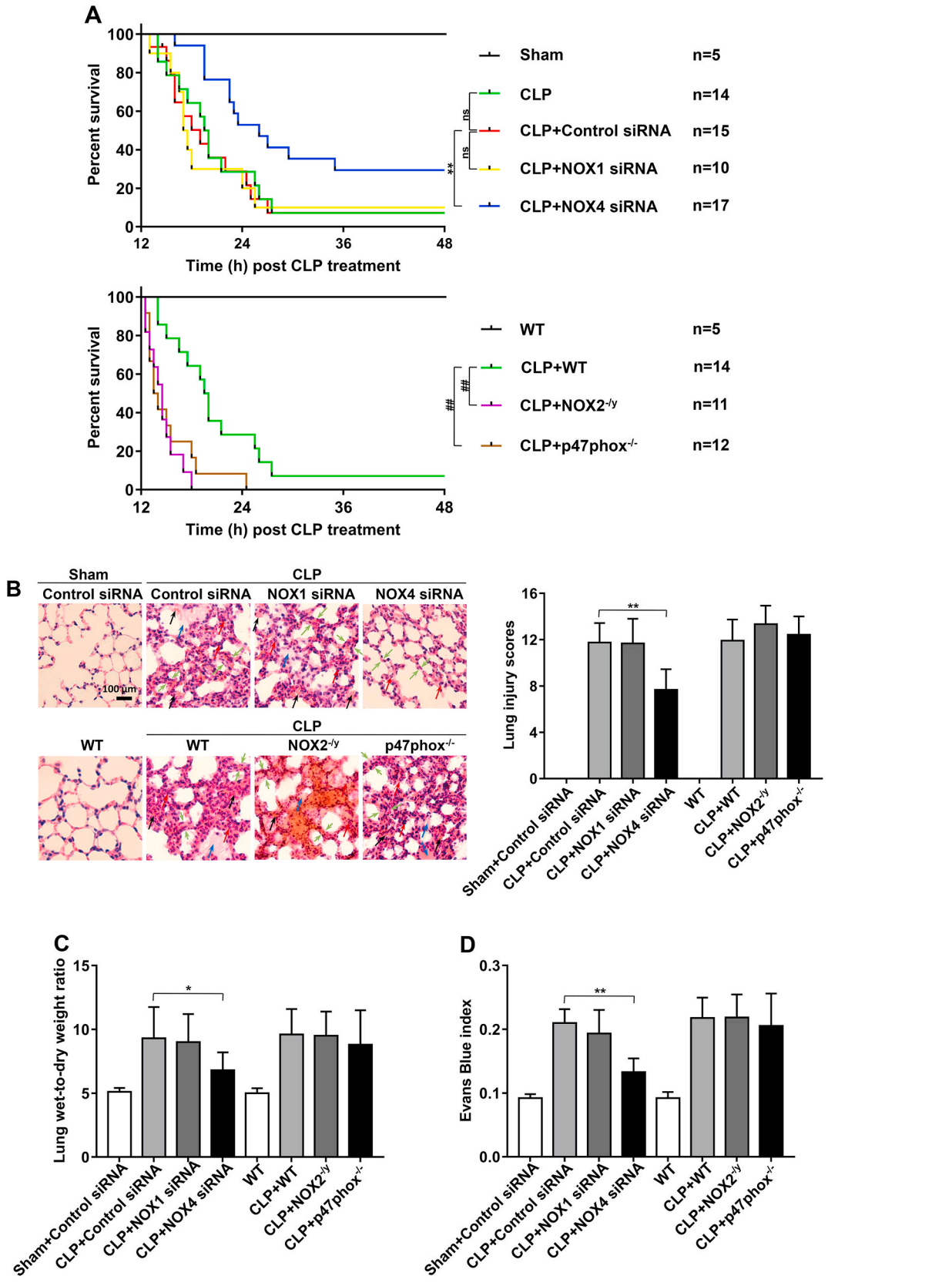

(caption on next page)

Fig. 1. NOX4 knockdown markedly improves survival and attenuates acute lung injury in CLP-induced septic mice. Sepsis was induced by cecal ligation and puncture (CLP) in wild-type (WT) mice and mice deficient in NOX2 or p47phox, or mice transfected of control siRNA, NOX1 or NOX4 siRNA. Natural death time was recorded by observation every 30 min starting 12 h after CLP, and the death time was presented as a Kaplan-Meier plot using the Prism software, and log-rank test was used to compare survival between groups. Other mice were harvested at 16 h post CLP and lung tissues harvested for analyses of histomorphology, Evans Blue index and wet-to-dry weight ratio were used to assess severity of acute lung injury. **(A)** Survival curves in sham group, CLP groups treated with control siRNA, NOX1 or NOX4 siRNA, CLP WT group and CLP groups made in NOX2 or p47phox knockout mice. $^{**}p < 0.01$, $^{\#\#}p < 0.01$. **(B)** Representative images of H&E staining of lung tissue sections and semiquantitative histological scores of lung injury in experimental groups described in panel A. H&E stainings indicate signs of inflammation (red arrows), edema (blue arrows), hemorrhage (black arrows), and alveolar septal thickening (green arrows) from the cross sections of the lung. Bar = 100 μm. Data are presented as Mean±SEM, n = 5. $^{**}p < 0.01$ vs. CLP group. **(C–D)** Lung wet-to-dry weight ratio and Evans Blue index were determined in experimental groups as described in panel A. Data are presented as Mean±SEM, n = 5. $^{*}p < 0.05$, $^{**}p < 0.01$ vs. control siRNA transfected CLP group. Data indicate NOX4 knockdown in CLP mice is selectively and robustly effective in improving survival and attenuating acute lung injury. (For interpretation of the references to color in this figure legend, the reader is referred to the Web version of this article.)

The increased phosphorylation of CaMKII was significantly inhibited by NOX4 knockdown (Fig. 3B), while phosphorylation of ERK1/2 and MLCK, downstream targets of CaMKII, were also increased by CLP but inhibited by NOX4 knockdown (Fig. 3B).

As the downstream pathway, blocking of CaMKII is anticipated to correspondingly alleviate NOX4-mediated pulmonary hyperpermeability. Therefore, we next examined whether KN93, a selective inhibitor for CaMKII, could abolish CLP-induced pulmonary hyperpermeability. Mice were treated with either KN93 (0.05 mg/day/mouse) or KN92 (the inactive derivative of KN93, 0.05 mg/day/mouse) for 1 week prior to CLP surgery. Of note, the upstream production of superoxide by DHE imaging was not affected by CaMKII inhibition (Fig. 3C). The increased CaMKII phosphorylation was however effectively abrogated by KN93 treatment (Fig. 3D). As shown in Fig. 3E and F, the increased lung wet-to-dry ratio and Evans Blue index were all attenuated in KN93 treated CLP mice, which are consistent to the effects of NOX4 knockdown. The negative control compound KN92 however had no effects on any of responses (Fig. 3E–F). These data demonstrate that CaMKII/ERK1/2/MLCK pathway is involved in NOX4-mediated pulmonary hyperpermeability in CLP-induced sepsis.

3.4. NOX4 knockdown preserves expression of endothelial tight junction proteins ZO-1 and Occludin in CLP-induced septic mice

To explore endothelial barrier function in CLP-induced septic mouse lungs, we examined expression of tight junction proteins ZO-1 and Occludin in CLP treated mice. As shown in Fig. 4A, protein expression of ZO-1 and Occludin was markedly downregulated after CLP, while NOX4 knockdown significantly restored protein abundance of ZO-1 and Occludin (Fig. 4A). Immunohistochemistry (Fig. 4B) and immunofluorescence (Fig. 4C) analyses were used to further verify the results of Western blotting in Fig. 4A, and the results consistently demonstrate a remarkab restoration of ZO-1 and Occludin expression by NOX4 knockdown. These results indicate a causal role of NOX4 in inducing tight junction protein deficiency in CLP mice.

3.5. Pharmacological scavenging of ROS by TEMPO displayed similar effects with NOX4 knockdown in protection against pulmonary hyperpermeability in CLP-induced septic mice

Mice were pretreated with TEMPO (100 mg/kg), a membrane-permeable superoxide scavenger, for 1 h prior to CLP to evaluate whether scavenging ROS displays similar effects with NOX4 knockdown in protection against pulmonary hyperpermeability. As shown in Fig. 5A, CLP significantly increased DHE fluorescent intensity in lung tissue sections, which was substantially attenuated by TEMPO treatment. In addition, CLP increased lung wet-to-dry ratio and Evans Blue index, all of which were markedly abrogated by treatment with TEMPO (Fig. 5B–C). Therefore, these data indicate that TEMPO scavenging of superoxide exerts similar protective effects on ALI as NOX4 knockdown did.

3.6. NOX4 knockdown attenuates LPS-induced endothelial permeability via CaMKII/ERK1/2/MLCK pathway inactivation

Endothelial barrier dysfunction is a key pathological feature of ALI, inhibition of which can prevent disease progression. We next evaluated whether NOX4 knockdown in cultured human pulmonary microvascular endothelial cells (HPMECs) could similarly reverse LPS induced endothelial barrier dysfunction. As shown in Fig. 6A, NOX4 siRNA transfection effectively attenuated NOX4 protein abundance in HPMECs. We next examined effects of NOX4 knockdown on barrier function in HPMECs by monitoring changes in Transendothelial Electrical Resistance (TEER) values using an electrical cell substrate impedance sensing system (ECIS) for 8 h after LPS (1 μg/ml) treatment of endothelial cells. The ECIS is an established impedance-based cell-monitoring platform to measure endothelial cell monolayer integrity and permeability [35]. Of note, LPS exposure induced decreased TEER values in HPMECs, which was significantly reversed by NOX4 siRNA (Fig. 6B), indicating a protective effect on barrier integrity of NOX4 inhibition.

Considering the critical role of ROS in LPS-induced increases in endothelial permeability, DHE imaging for determination of superoxide production was performed in HPMECs with or without NOX4 knockdown. Of note, NOX4 knockdown abolished ROS production in response to LPS treatment (Fig. 6C).

We next examined the activities of CaMKII/ERK1/2/MLCK pathway in LPS-treated HPMECs. Results indicate that LPS increased phosphorylation of CaMKII at Thr-286 in a time-dependent manner (Fig. 6D). The upregulated phosphorylation of CaMKII was inhibited by NOX4 siRNA (Fig. 6E), as was phosphorylation of the downstream effectors, ERK1/2 and MLCK (Fig. 6E).

To evaluate whether inhibition of CaMKII is effective in alleviating NOX4-mediated endothelial cell barrier dysfunction in HPMECs, we next assessed whether KN93, a selective inhibitor of CaMKII, could abolish LPS-induced endothelial hyperpermeability. Of note, the upstream production of superoxide detected by DHE imaging was not affected by CaMKII inhibition (Fig. 6F), whereas LPS-induced increases in CaMKII was substantially attenuated by KN93 treatment (Fig. 6G). As shown in Fig. 6H, TEER values were significantly decreased in LPS-treated HPMECs, while KN93 treatment significantly alleviated this response. These data indicate that CaMKII inhibition protects against LPS-induced endothelial barrier dysfunction in HPMECs.

We next examined potential effects of NOX4 knockdown on the expression of tight junction proteins ZO-1 and Occludin in LPS-treated HPMECs. Consistent to in vivo findings, protein expression of ZO-1 and Occludin was significantly downregulated in LPS treated cells, while NOX4 knockdown restored the protein abundance of ZO-1 and Occludin (Fig. 6I). In addition, immunofluorescent staining also showed that NOX4 knockdown significantly reversed LPS-induced reductions in ZO-1 protein abundance (Fig. 6J). These data demonstrate that CaMKII/ERK1/2/MLCK pathway is involved in NOX4-dependentbarrier dysfunction in LPS-treated HPMECs.

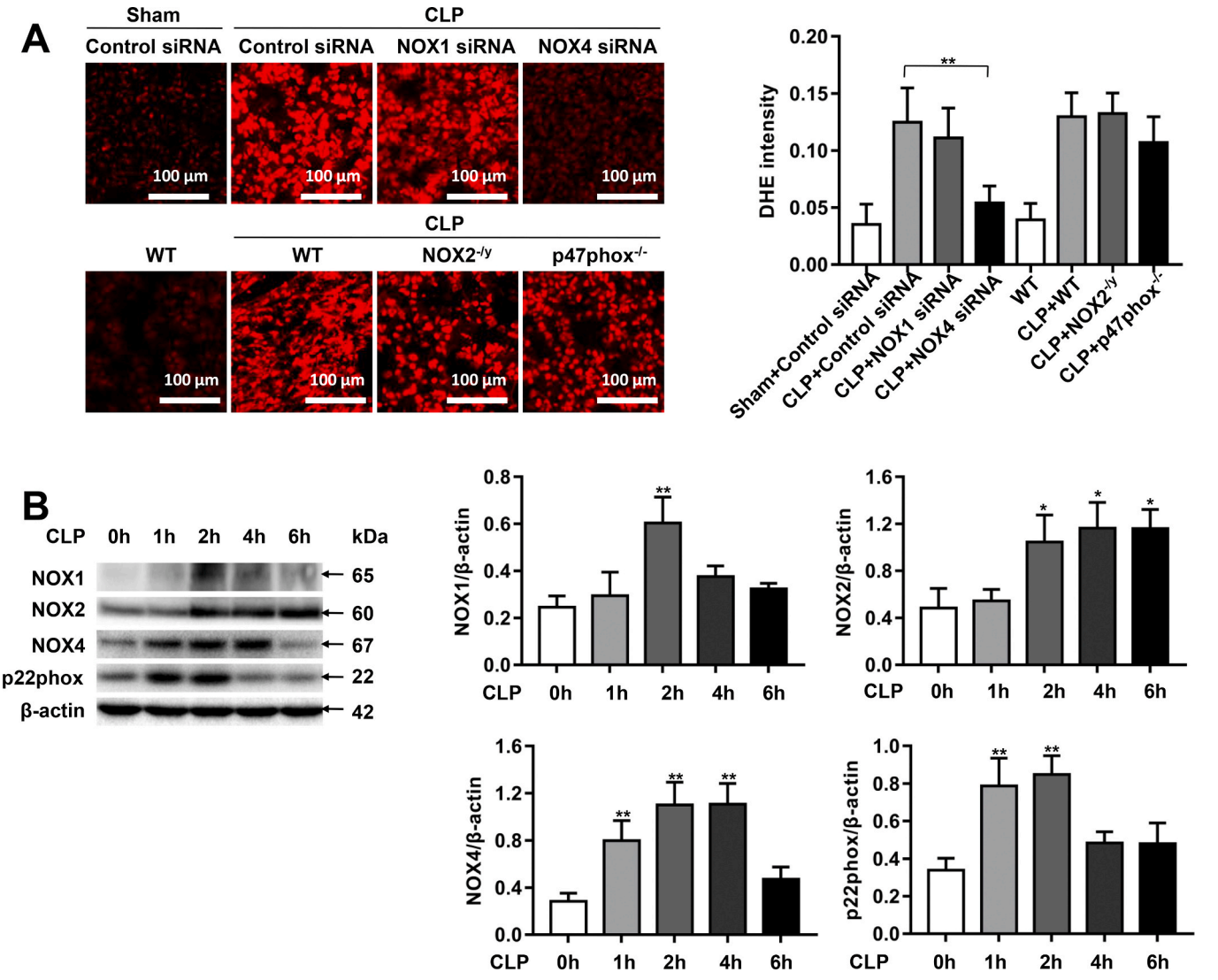

Fig. 2. NOX4 knockdown decreases ROS production in CLP-induced septic mice. Sepsis was induced by CLP in wild-type (WT) mice and mice deficient in NOX2 or p47phox, or mice transfected of control siRNA, NOX1 or NOX4 siRNA. Mouse lung tissues were freshly harvested at 16 h post CLP for DHE fluorescent imaging, or at 1, 2, 4, 6 h post CLP for Western blotting analyses. **(A)**: Representative images of DHE fluorescent imaging of lung tissue sections in sham group, CLP groups treated with control siRNA, NOX1 or NOX4 siRNA, CLP WT group and CLP groups made in NOX2 or p47phox knockout mice. Freshly prepared lung OCT sections were incubated with DHE (2 μmol/L) in the dark for 30 min, and fluorescent images were captured using a Nikon A1R Confocal Microscope. Photographs were taken at ×200 magnification. Data are presented as Mean±SEM. n = 10. **p < 0.01 vs. CLP group. **(B)** Representative Western blots and quantitative data of NOX1, NOX2, NOX4 and p22phox protein expression in mice at 1, 2, 4, 6 h post CLP. Data are presented as Mean±SEM; n = 3. *p < 0.05, **p < 0.01 vs. 0 h group. **(C)** Representative Western blots and quantitative data of NOX1, NOX2, NOX4, and p22phox expression in lung tissues of control siRNA or NOX1 siRNA treated mice with or without CLP for 2 h, indicating that NOX1 siRNA attenuated the expression of NOX1, while having no effects on the expression of NOX2, NOX4, and p22phox. Data are presented as Mean±SEM; n = 3. **p < 0.01. **(D)** Representative Western blots and quantitative data of NOX1, NOX2, NOX4, and p22phox expression in lung tissues of WT and NOX2 knockout mice with or without CLP for 2 h, indicating that NOX2 knockout had absence of NOX2 but upregulated expression of NOX4 and p22phox. Data are presented as Mean±SEM; n = 3. **p < 0.01. **(E)** Representative Western blots and quantitative data of NOX1, NOX2, NOX4, and p22phox in lung tissues of control siRNA or NOX4 siRNA treated mice with or without CLP for 2 h, indicating that NOX4 siRNA attenuated the expression of NOX4 and p22phox, while having no effect on the protein expression of NOX1 and NOX2. Data are presented as Mean±SEM; n = 3. **p < 0.01. **(F)** Representative Western blots and quantitative data of p47phox and p22phox in lung tissues of WT or p47phox knockout mice with or without CLP for 2 h, indicating that p47phox knockout had absence of p47phox but upregulated expression of p22phox. Data are presented as Mean±SEM; n = 3. *p < 0.05.

3.7. Pharmacological scavenging of ROS by TEMPO displayed similar effects with NOX4 knockdown in protection against LPS-induced barrier dysfunction in HPMECs

To examine whether LPS induced endothelial barrier dysfunction in HPMECs is mediated by increased ROS production, cells were pretreated with TEMPO (0.1 mmol/L) for 1 h prior to LPS treatment. As shown in Fig. 7A, LPS significantly elevated DHE fluorescent intensity in endothelial cells indicating increased ROS production, which was however substantially attenuated by TEMPO treatment. Further, we assessed the effects of TEMPO on LPS-induced endothelial barrier dysfunction by measuring TEER values using the ECIS system. As shown in Fig. 7B, LPS markedly increased endothelial permeability and reduced TEER value, which was substantially alleviated by TEMPO treatment. These results indicate that scavenging ROS with TEMPO has similar effects with NOX4 knockdown in HPMECs in protecting against endothelial barrier dysfunction.

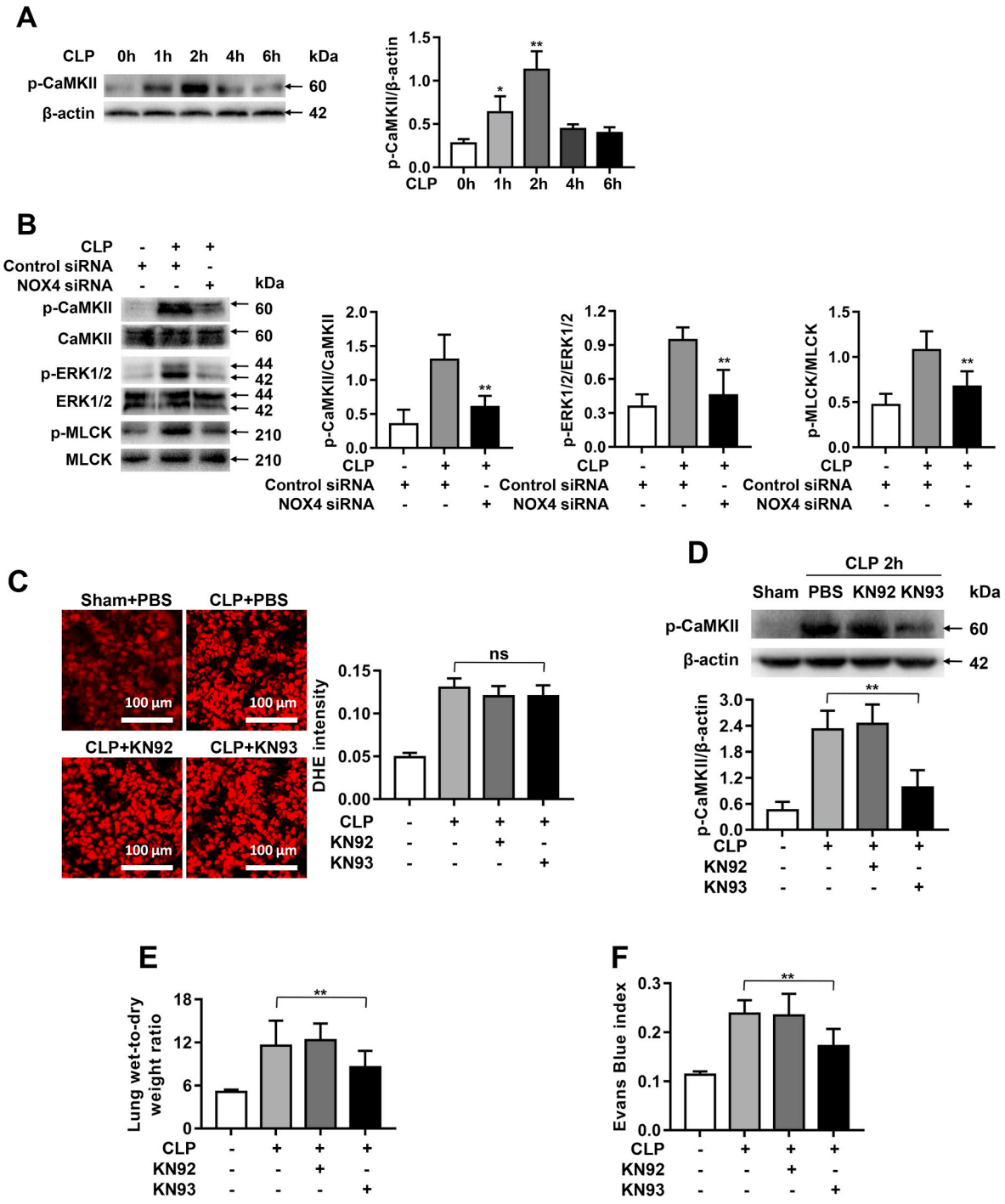

Fig. 3. NOX4 knockdown prevents CLP-induced pulmonary hyperpermeability via CaMKII/ERK1/2/MLCK pathway inactivation. Sepsis was induced by CLP in mice transfected of control siRNA or NOX4 siRNA. Mouse lung tissues were harvested at 1, 2, 4, 6 h post CLP for Western blotting analyses. In parallel experiments, septic mice were pretreated with either KN93 (0.05 mg/day/mouse) or KN92 (0.05 mg/day/mouse) for 1 week before exposure to CLP for 16 h to examine effects of KN93 on pulmonary hyperpermeability in CLP-treated mice. **(A)**: Representative Western blots and quantitative data of CaMKII phosphorylation in mouse lung tissues at 1, 2, 4, 6 h post CLP. Data are presented as Mean±SEM; n = 3. *$p < 0.05$, **$p < 0.01$ vs. 0 h group. **(B)**: Representative Western blots and quantitative data of CaMKII, ERK1/2, and MLCK phosphorylation in sham mice or CLP treated mice transfected of control siRNA or NOX4 siRNA. Results indicate NOX4 knowdown markedly attenuated phosphorylation of CaMKII, ERK1/2 and MLCK. Data are presented as Mean±SEM; n = 3. **$p < 0.01$ vs. Control-CLP group. **(C)**: Representative fluorescent images of DHE detection of ROS production in CLP mice with saline or KN92/KN93 treatment, indicating the upstream production of superoxide was not affected by CaMKII inhibition KN93. Data are presented as Mean±SEM; n = 3. **(D)**: Representative Western blots and quantitative data of p-CaMKII expression in sham mice, or CLP treated mice pretreated with KN92 or KN93. Results indicate KN93 inhibition of CaMKII phosphorylation. Data are presented as Mean±SEM; n = 3. **$p < 0.01$. **(E–F)**: Lung wet-to-dry weight ratio and Evans Blue index were determined in PBS or KN92/KN93 treated CLP mice, indicating attenuation of pulmonary hyperpermeability by KN93 treatment in vivo. Data are presented as Mean±SEM, n = 5. **$p < 0.01$ vs. CLP group. (For interpretation of the references to color in this figure legend, the reader is referred to the Web version of this article.)

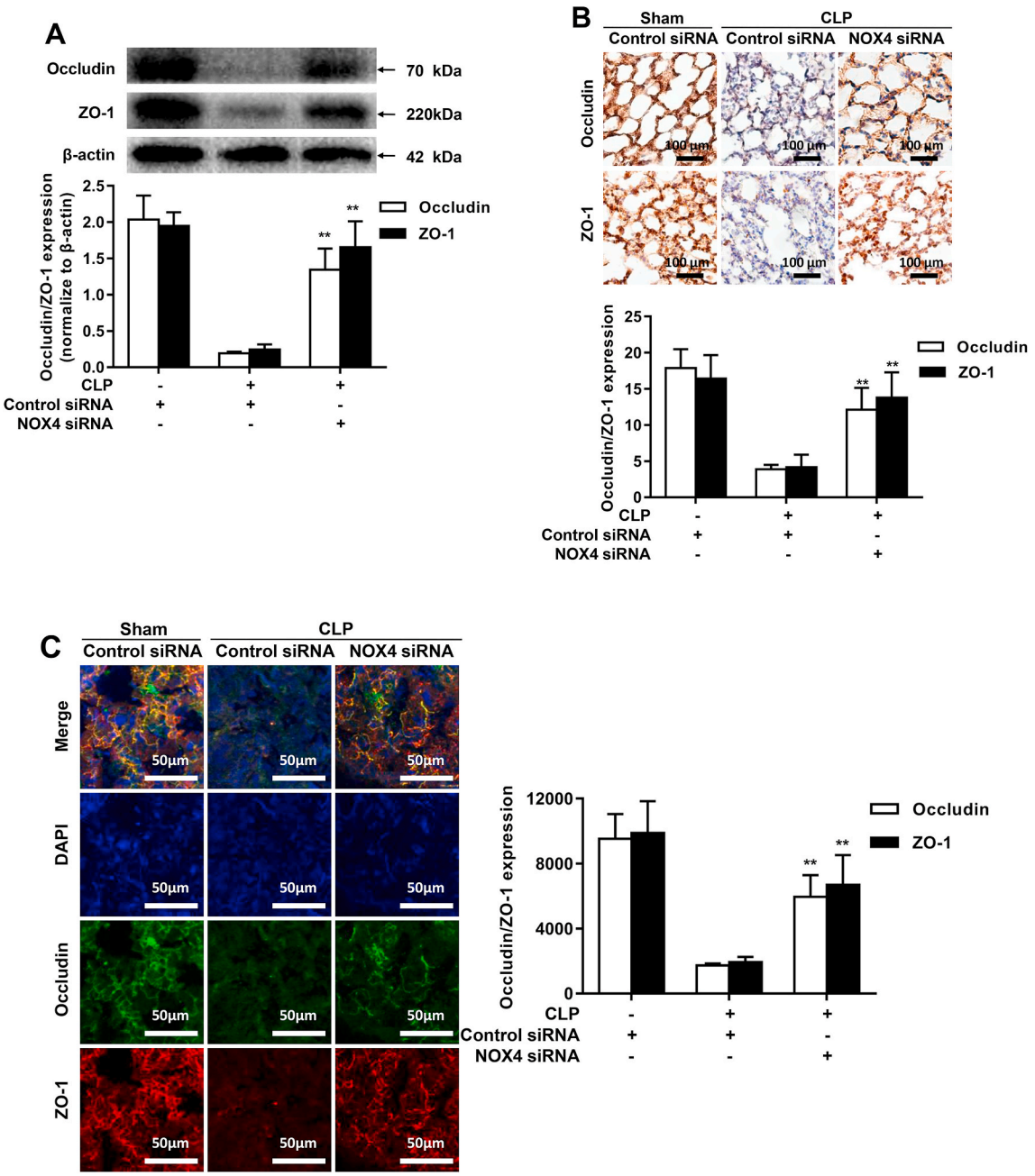

Fig. 4. NOX4 knockdown preserves expression of endothelial tight junction proteins ZO-1 and Occludin in CLP-induced septic mice. Sepsis was induced by CLP in mice transfected of control siRNA or NOX4 siRNA. Mouse lung tissues were harvested at 16 h post CLP for Western blotting, immunohistochemical or immunofluorescent analyses. **(A)**: Representative Western blots and quantitative data of Occludin and ZO-1 protein expression in sham mice or CLP treated mice transfected of control siRNA or NOX4 siRNA. Data are presented as Mean±SEM; n = 3; **p < 0.01 vs. CLP group. **(B)**: Representative immunohistochemical staining images of Occludin and ZO-1 in lung paraffin sections. Dark brown dots indicate positively stained cells. Morphometric analysis of immunostained area for each protein in relation to total area was performed quantitatively using Image-Pro Plus software. Scale bars: 100 μm. Data are presented as Mean±SEM. n = 3. *p < 0.05, **p < 0.01 vs. control siRNA transfected CLP group. **(C)**: Representative immunofluorescent staining images of Occludin and ZO-1 in lung OCT sections. Cryosections of lung were stained for Occludin (green), ZO-1 (red) and DAPI (blue). The fluorescent images were captured using a Nikon A1R confocal microscope. Densities of Occludin and ZO-1 fluorescence were quantified using the Image J software. Scale bars: 50 μm. Data are presented as Mean±SEM; n = 3. *p < 0.05, **p < 0.01 vs. Control siRNA transfected CLP group. Results from A-C indicate that NOX4 knockdown markedly reversed CLP-induced deficiencies in ZO-1 and Occludin expression. (For interpretation of the references to color in this figure legend, the reader is referred to the Web version of this article.)

4. Discussion

In the present study, we examined potential critical roles of NOX isoforms in mediating pulmonary endothelial barrier dysfunction to result in lung injuries and death in response to CLP-induced sepsis. Our work identifies a novel pathway, exclusive to NOX4 but not other NOX isoforms, in mediating endothelial cell barrier dysfunction and lung hyperpermeability during preclinical ALI/ARDS. NOX4-mediated injury occurs via production of ROS, redox-sensitive activation of CaMKII/ERK1/2/MLCK pathway, and consequent loss in tight junction proteins, ZO1 and Occludin. Targeting NOX4, scavenging superoxide radicals, or inhibiting CaMKII activation can block this pathway and relieve endothelial barrier dysfunction and lung injuries in CLP mice. These new findings are illustrated in Fig. 8.

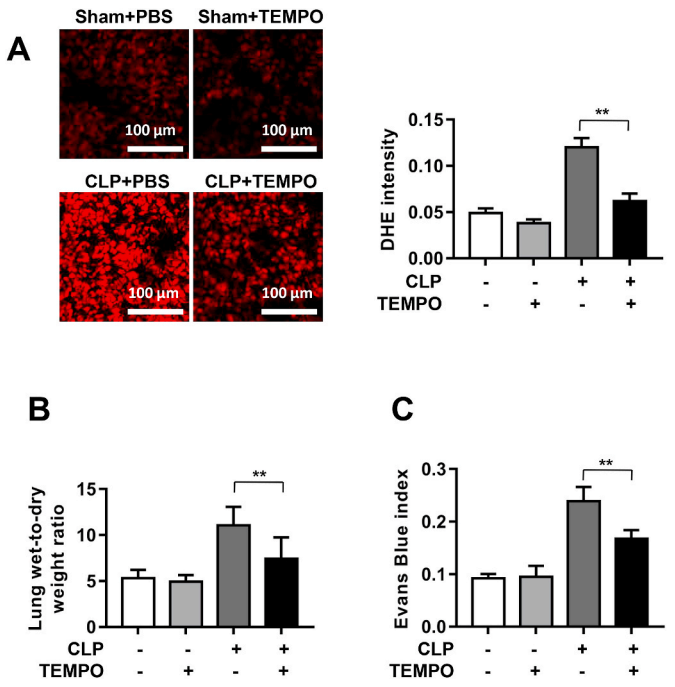

Fig. 5. Pharmacological scavenging of ROS by TEMPO displayed similar effects with NOX4 knockdown in protection against pulmonary hyperpermeability in CLP-induced septic mice. Mice were treated with TEMPO (superoxide scavenger; 100 mg/kg) or PBS for 1 h prior to induction of sepsis with CLP in mice transfected of control siRNA or NOX4 siRNA. Mice were harvested at 16 h post CLP and lung tissues harvested for DHE fluorescent imaging, lung wet-to-dry weight ratio and Evans Blue index to assess effects of TEMPO on severity of acute lung injury. **(A)**: Representative DHE fluorescent images of superoxide production in CLP mice with or without TEMPO treatment/ Data indicate that TEMPO substantially attenuated CLP induced increase in ROS production. Photographs were taken at ×200 magnification. Data are presented as Mean±SEM; n = 10. **p < 0.01 vs. CLP group. **(B–C)**: Lung wet-to-dry weight ratio and Evans Blue index were determined in PBS or TEMPO treated CLP mice Data indicate that TEMPO treatment markedly attenuated acute lung injury in CLP mice in vivo. Data are presented as Mean±SEM, n = 5. **p < 0.01 vs. CLP group. (For interpretation of the references to color in this figure legend, the reader is referred to the Web version of this article.)

NOX4-dependent activation of CaMKII/ERK1/2/MLCK pathway led to vascular leakage characterized by increased lung wet-to-dry ratio and Evans Blue index in ALI. In vivo RNAi knockdown of NOX4, rather than genetic ablation of NOX1, NOX2 or p47phox, substantially improved survival, which was accompanied by reversed lung injuries characterized by edema, hemorrhage, alveolar septal thickening, and inflammatory cell infiltration. NOX4 knockdown in vivo alleviated sepsis-induced oxidative stress, attenuated redox-sensitive activation of CaMKII/ERK1/2/MLCK pathway, and restored protein expression of endothelial cell tight junction ZO-1 and Occludin, resulting protection against endothelial barrier dysfunction, lung injuries and mortality. Scavenging superoxide with TEMPO, or inhibiting CaMKII activation with KN93, exerted similar results as NOX4 knockdown. In addition, NOX4 knockdown in HPMECs restored endothelial barrier function via inactivation of redox-sensitive CaMKII/ERK1/2/MLCK pathway. These data clearly indicate that targeting NOX4 may prove effective in treating CLP-induced ALI by attenuating redox-sensitive activation of CaMKII/ERK1/2/MLCK pathway to preserve EC barrier function.

Accumulating evidence has shown that different NOX isoforms have differential roles in the pathogenesis of different cardiometabolic diseases [15]. For instance, NOX1 has been shown to mediate diabetic endothelial dysfunction, and endothelial cell ROS production in response to atherogenic oscillatory shear stress [18,36,37]. On the contrary, NOX4 plays a critical role in cardiac ischemia-reperfusion injury [38]. However, both NOX1 and NOX2 were found involved in Ang II induced hypertension [39,40]. Nonetheless, roles of NOX isoforms in the pathogenesis of respiratory diseases are less studied or fully understood. The current study identified a novel and selective role of NOX4 in the endothelial cell responses to severe inflammatory activations in a preclinical model of CLP-induced ALI. Results indicate that inhibition of NOX4, rather than that of NOX1, NOX2 or p47phox, substantially improved survival of the CLP-treated mice and reduced lung injuries. It has been recognized that endothelial barrier dysfunction plays a major role in ALI/ARDS [4–7]. In this study, we found that siRNA knockdown of NOX4 markedly abrogated lung wet-to-dry ratio, and Evans Blue index in CLP-induced septic mice. These data demonstrate that NOX4, rather than NOX1 or NOX2, plays a critical role in mediating sepsis-induced pulmonary hyperpermeability to mediate lung injuries in a CLP-induced ALI model. Of note, p47phox knockout mice had similar phenotype as of NOX1 knockdown or NOX2 knockout mice in failing to protect against CLP-induced septic ALI. This is consistent with the notion that p47phox is involved in activating both NOX1 and NOX2 isoforms [18].

Increased ROS generation in lung endothelial cells during ALI has been shown to play a major role in inducing loss of barrier integrity [11,15]. ROS participate in the modulation of cell-signaling pathways which activate key transcription factors, such as NF-κB, resulting in further deterioration of inflammatory responses [41]. In the present study, we assessed ROS production using DHE fluorescent imaging in CLP-stimulated control siRNA treated/WT mice and mice deficient in NOX isoforms. Results indicate that CLP rapidly increased ROS production in the mouse lung, which was substantially abrogated by in vivo RNAi mediated NOX4 knockdown. Whereas NOX1 knockdown, NOX2 knockout, or p47phox knockout had no effects on ROS production in CLP-treated mouse lungs. *In vitro* studies consistently showed that NOX4 knockdown significantly attenuated LPS-induced increase in ROS production in HPMECs. Of note, whereas RNAi based NOX1 and NOX4 knockdown had no effects on the expression of other NOX isoforms in mouse lung tissues, NOX2 knockout led to increased expression of NOX4 and p22phox under CLP condition, which may at least in part explain that NOX2 knockout had aggravated oxidative stress and lung injury (0% survival rate vs. 28.6% in WT control mice). Likewise, p47phox knockout in CLP treated mice also resulted in upregulation of p22phox, and displayed worse survival rate and lung injury (8.3% survival rate vs 28.6% in WT control mice). In line with our results, it was shown that p47phox or NOX2 knockout leads to compensatory upregulation of NOX4 in cigarette smoke exposed mouse lung [42]. In the present study, we observed a co-inhibition of p22phox with NOX4 knockdown, which may additionally contribute to the beneficial effects of NOX4 knockdown.

CaM Kinase II is redox-sensitively activated to mediate microvascular barrier dysfunction via ERK1/2/MLCK pathway [21,22,24]. Phosphorylation at Thr-286 in the autoinhibitory domain of CaMKII prevents re-association of the kinase domain to result in persistent CaMKII activation [21,22,24]. In our study, we found a significant increase in CaMKII Thr-286 phosphorylation in CLP mice and LPS-stimulated endothelial cells, which can be inhibited by NOX4 knockdown. ERK1/2 and MLCK [24,43–46], downstream effectors of CaMKII, also exhibited increased phosphorylation in CLP mice and LPS-stimulated endothelial cells, which were significantly abrogated by NOX4 knockdown and the pharmacological inhibitor of CaMKII, KN93. Therefore, phosphorylation-dependent activation of CaMKII and its downstream effectors underlies NOX4-dependent modulation of lung permeability. We believe that this role of redox-sensitive activation of CaMKII/ERK1/2/MLCK pathway is selective to NOX4 activation, as only specific knockdown of NOX4 was able to improve survival and reverse lung injuries that are subsequent to CaMKII/ERK1/2/MLCK-dependent induction of EC barrier dysfunction.

Tight junctions between HPMECs help to form the barrier to keep normal barrier function. Tight junctions are intercellular structures that

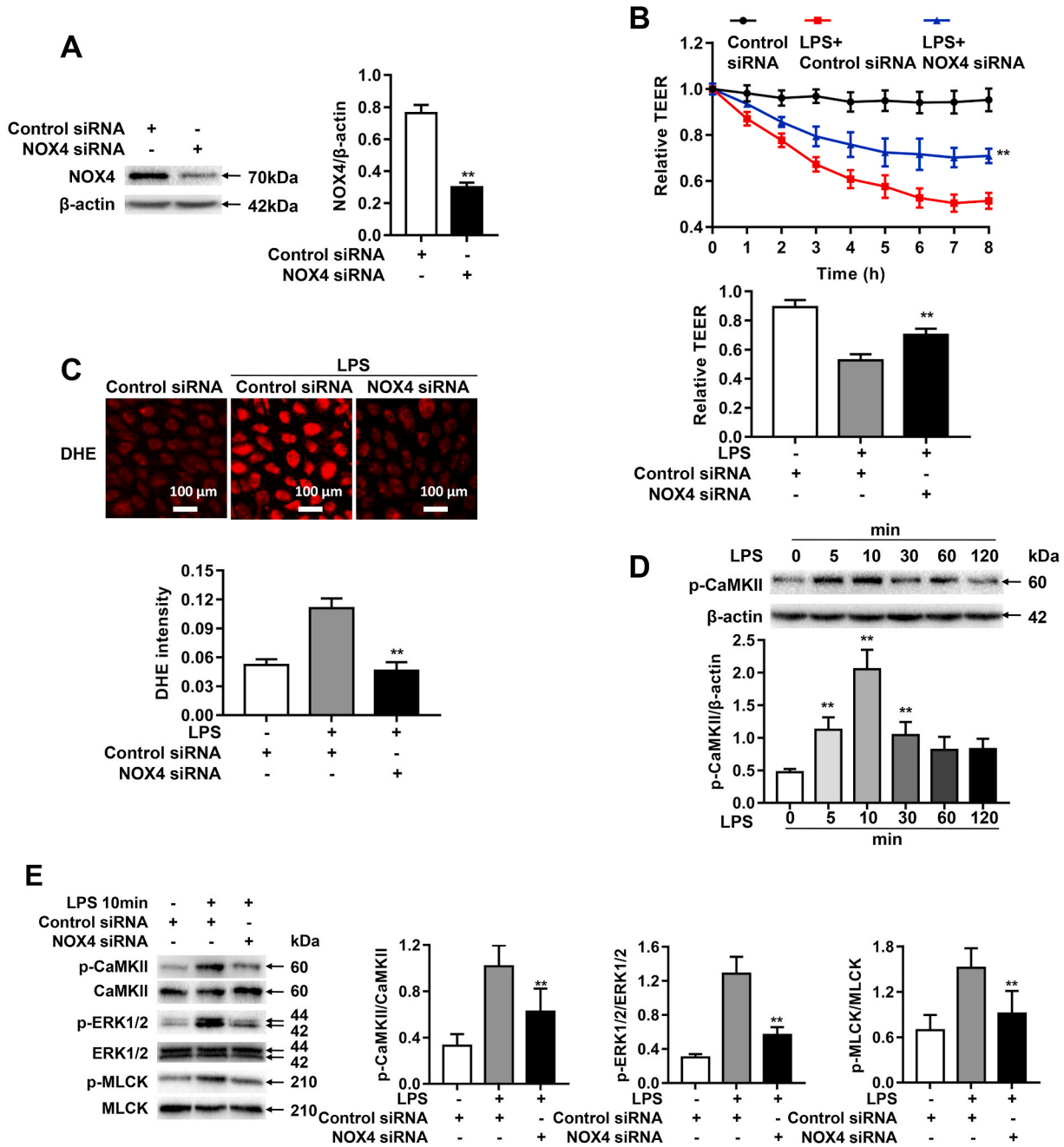

Fig. 6. NOX4 knockdown attenuates LPS-induced endothelial permeability via CaMKII/ERK1/2/MLCK pathway inactivation. Sepsis was mimicked *in vitro* by LPS (1 μg/ml) stimulation in HPMECs pre-transfected with control siRNA or NOX4 siRNA. **(A)**: Representative Western blots and quantitative data of NOX4 protein expression in HPMECs transfected with control siRNA or NOX4 siRNA, indicating that NOX4 siRNA transfection effectively attenuated NOX4 protein abundance. Data are presented as Mean±SEM. n = 3. **p < 0.01. **(B)**: Changes in TEER values in real time following LPS treatment up to 8 h. Data indicate that NOX4 knockdown substantially alleviated LPS induced decrease in TEER values in HPMECs. Data are presented as Mean±SEM. n = 6–9, **p < 0.01 vs. control siRNA transfected LPS group. **(C)**: Representative images of DHE staining of HPMECs in control group or LPS treated groups transfected with control siRNA or NOX4 siRNA, indicating that NOX4 knockdown completely abrogated ROS production in response to LPS treatment. Cells were incubated with DHE (2 μM) in the dark for 30 min, and fluorescent images were captured using a Nikon A1R Confocal Microscope. Photographs were taken at ×200 magnification. Data are presented as Mean±SEM. n = 3. **p < 0.01 vs. control siRNA transfected LPS group. **(D)**: Representative Western blots and qualitative data of CaMKII phosphorylation in HPMECs following LPS challenge, indicating a time-dependent increase. Data are presented as Mean±SEM. n = 3. **p < 0.01 vs. 0 h group. **(E)**: Representative Western blots and quantitative data of CaMKII, ERK1/2, and MLCK phosphorylation in control or LPS (1 μg/ml) treated HPMECs transfected of control siRNA or NOX4 siRNA. Results indicate that NOX4 knockdown inactivated CaMKII/ERK1/2/MLCK pathway in LPS-treated HPMECs. Data are presented as Mean±SEM; n = 3. *p < 0.05, **p < 0.01 vs. control siRNA transfected LPS group. Results in F–H indicate that pharmacological inhibition of CaMKII is protective endothelial barrier dysfunction in LPS treated HPMECs. Cells were incubated with either KN93 (1 μmol/L) or KN92 (1 μmol/L) for 24 h and then exposed to LPS (1 μg/ml) for 2 h. **(F)**: Representative fluorescent images of DHE detection of ROS production in LPS treated HPMECs with KN92 or KN93 treatment. Data indicate that the upstream production of superoxide was not affected by CaMKII inhibition KN93. Data are presented as Mean±SEM; n = 3. **(G)**: Representative Western blots and quantitative data of p-CaMKII expression in control HPMECs, or LPS stimulated HPMECs pre-treated with KN92 or KN93. KN93 attenuated CaMKII phosphorylation while KN92 had no effects. Data are presented as Mean±SEM; n = 3. **p < 0.01 vs. LPS group. **(H)**: Changes in TEER values in real time in LPS-stimulated HPMECs pre-treated with KN92 or KN93. Data indicate that KN93 treatment markedly preserved TEER values in LPS-treated HMPECs. Data are presented as Mean±SEM. n = 6–9, **p < 0.01 vs. LPS group. **(I)**: Representative Western blots and quantitative data of Occludin and ZO-1 expression in control HPMECs or LPS (1 μg/ml) stimulated HPMECs transfected with control siRNA or NOX4 siRNA. Data are presented as Means±SEM. n = 3. **p < 0.01 *vs.* LPS group. **(J)**: Representative immunofluorescent analysis of ZO-1

expression in control HPMECs or LPS (1 μg/ml) stimulated HPMECs transfected with control siRNA or NOX4 siRNA. Cells were grown on a glass chamber slid to confluence and then challenged with LPS (1 μg/ml) for 6 h. Immunofluorescent staining of ZO-1 (red), and nuclei (blue) was imaged by a Nikon A1R Confocal microscope. Scale bars: 100 μm. Data are presented as Means±SEM. n = 3. **p < 0.01 vs. LPS group. Results in (I–J) indicate that NOX4 knockdown preserved protein abundance of Occudin and ZO-1 following LPS stimulation. (For interpretation of the references to color in this figure legend, the reader is referred to the Web version of this article.)

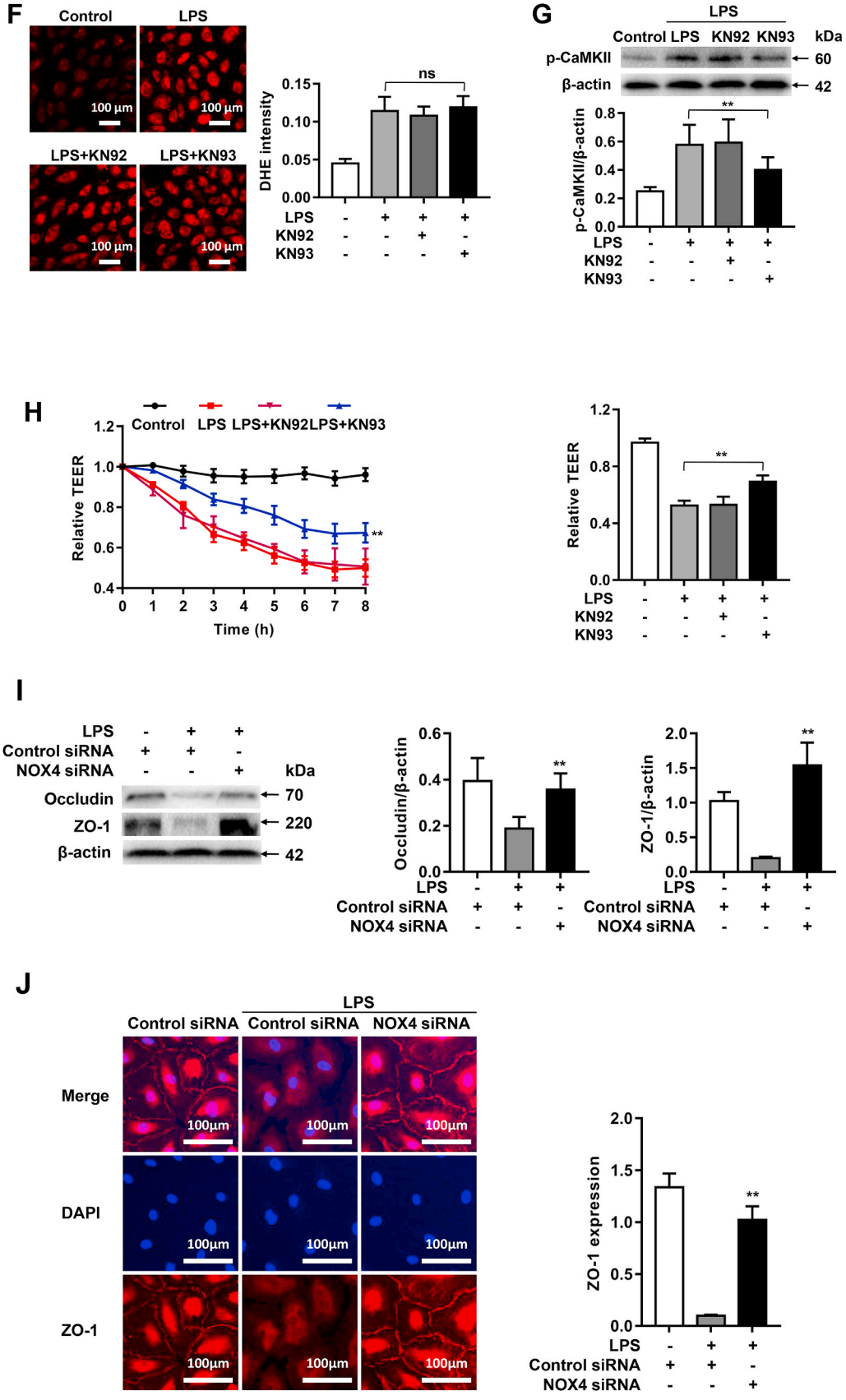

Fig. 6. (*continued*).

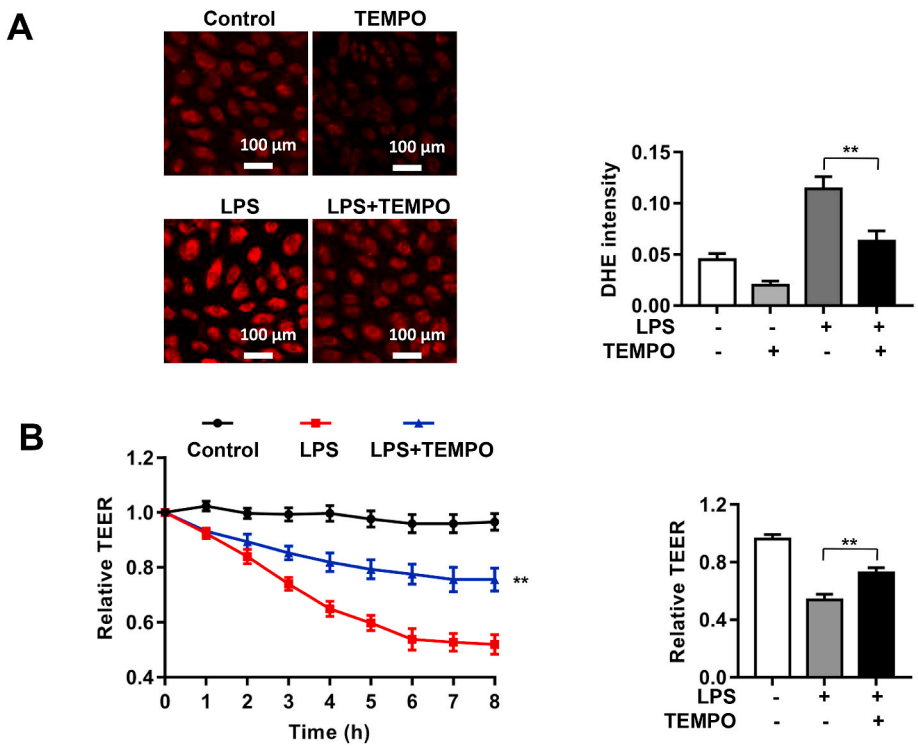

Fig. 7. Pharmacological scavenging of ROS by TEMPO displayed similar effects with NOX4 knockdown in protection against LPS-induced barrier dysfunction in HPMECs. HPMECs were transfected with control siRNA or NOX4 siRNA, and then treated with TEMPO (0.1 mmo/L) for 1 h prior to LPS (1 μg/ml) stimulation. Cells were incubated in ECIS for real time monitoring of changes in TEER values up to 8 h, or harvested at 2 h post LPS for DHE fluorescent imaging of ROS production. **(A)**: Representative DHE fluorescent images of superoxide production in LPS treated HPMECs with or without TEMPO treatment. Data indicate that TEMPO substantially attenuated LPS induced ROS production. Photographs were taken at ×200 magnification. Data are presented as Mean±SEM; n = 5. **p < 0.01 vs. LPS group. **(B)**: Changes in TEER values after TEMPO treatment in LPS exposed HPMECs. Data indicate that TEMPO treatment markedly abrogated LPS induced decline in TEER values. Data are presented as Means±SEM. n = 6–9. **p < 0.01 vs. LPS group.

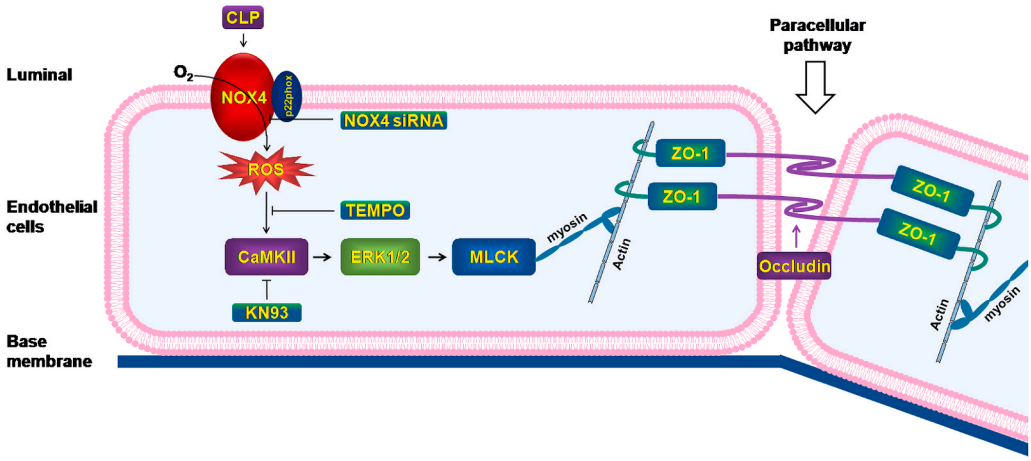

Fig. 8. Targeting NOX4 alleviates sepsis-induced acute lung injury via attenuation of redox-sensitive activation of CaMKII/ERK1/2/MLCK and endothelial cell barrier dysfunction. During ALI/ARDS, activation of NOX4, rather than other NOX isoforms, produces ROS and redox-sensitively activates CaMKII/ERK1/2/MLCK pathway to result in endothelial cell tight junction deficiency and barrier dysfunction, leading to acute lung injury and death in CLP-induced septic mice. RNAi inhibition of NOX4, scavenging superoxide radicals, or pharmacological inhibition of CaMKII can block this pathway and relieve endothelial cell barrier dysfunction and lung injuries in CLP mice. Targeting NOX4 may therefore prove to an innovative therapeutic option that is markedly effective in treating ALI/ARDS.

prevent the passage of molecules through the paracellular spaces [47,48]. They are composed of transmembrane proteins such as Occludin, claudins, tricellulin and other junction adhesion molecules (JAM), as well as cytoplasmic proteins such as ZOs, including ZO-1, ZO-2, ZO-3, which ultimately bind to the actin fibers of the cytoskeleton [47,48]. Importantly, preclinical studies have shown that tight junctions can be altered by the activation of different protein kinases, such as Ras homolog gene family member A (RhoA) [27], mitogen-activated protein kinase (MAPK) [27], as well as CaM Kinase II (CaMKII) [49]. In the present study, protein abundance of ZO-1 and Occludin was found markedly downregulated in CLP-treated mouse lungs, which was significantly alleviated by NOX4 knockdown. Moreover, NOX4 knockdown in HPMECs markedly reversed LPS-induced reduction in ZO-1 and Occludin protein expression. These results indicate that the injurious role of NOX4 activation in ALI is mediated by tight junction protein deficiency.

To compare the efficacies of a superoxide scavenger TEMPO to the effects of NOX4 knockdown, CLP mice and LPS-treated HPMECs were also administered with TEMPO *in vivo* and *in vitro*. Results indicate that CLP treatment significantly increased lung wet-to-dry ratio and the Evans Blue index, which were markedly attenuated by TEMPO. *In vitro* results also indicate that TEMPO treatment effectively alleviated enhanced endothelial permeability assessed by reduced TEER values. These results indicate the beneficial effects of NOX4 knockdown is mimicked by TEMPO scavenging of ROS production.

In conclusion, our data for the first time reveal a novel, selective and causal role of NOX4 activation in mediating EC barrier dysfunction, lung injuries and mortality in a preclinical model of CLP-induced sepsis, as well as in mediating LPS-induced EC barrier dysfunction in LPS-treated HPMECs. The beneficial effects of NOX4 inhibition are mediated by

attenuation of redox-sensitive activation of the CaMKII/ERK1/2/MLCK pathway, and restoration of endothelial tight junction proteins ZO-1 and Occudin. In contrast, inhibition of NOX1 or NOX2 was not effective in protecting against septic ALI in CLP mice. These findings indicate that targeting NOX4 and its downstream signaling pathways may prove to be an innovative therapeutic strategy for the treatment of ALI/ARDS.

Acknowledgements

This work was supported by the National Key Research and Development Program of China Grant 2016YFC1303900 (CW), and a UCLA Research Fund (HC).

Transparency document

Transparency document related to this article can be found online at https://doi.org/10.1016/j.redox.2020.101638.

References

[1] M.A. Matthay, R.L. Zemans, The acute respiratory distress syndrome: pathogenesis and treatment, Annu. Rev. Pathol. 6 (2011) 147–163.
[2] E. Fan, D. Brodie, A.S. Slutsky, Acute respiratory distress syndrome: advances in diagnosis and treatment, JAMA 319 (2018) 698–710.
[3] G. Bellani, J.G. Laffey, T. Pham, E. Fan, L. Brochard, A. Esteban, L. Gattinoni, F. van Haren, A. Larsson, D.F. McAuley, M. Ranieri, G. Rubenfeld, B.T. Thompson, H. Wrigge, A.S. Slutsky, A. Pesenti, Epidemiology, patterns of Care, and mortality for patients with acute respiratory distress syndrome in intensive Care units in 50 countries, JAMA 315 (2016) 788–800.
[4] S.M. Dudek, J.G. Garcia, Cytoskeletal regulation of pulmonary vascular permeability, J. Appl. Physiol. (Bethesda, Md. 1985) 91 (2001) 1487–1500.
[5] B.J. McVerry, J.G. Garcia, Endothelial cell barrier regulation by sphingosine 1-phosphate, J. Cell. Biochem. 92 (2004) 1075–1085.
[6] L.B. Ware, M.A. Matthay, The acute respiratory distress syndrome, N. Engl. J. Med. 342 (2000) 1334–1349.
[7] D. Mehta, A.B. Malik, Signaling mechanisms regulating endothelial permeability, Physiol. Rev. 86 (2006) 279–367.
[8] M.A. Matthay, L.B. Ware, G.A. Zimmerman, The acute respiratory distress syndrome, J. Clin. Invest. 122 (2012) 2731–2740.
[9] S. Tasaka, F. Amaya, S. Hashimoto, A. Ishizaka, Roles of oxidants and redox signaling in the pathogenesis of acute respiratory distress syndrome, Antioxidants Redox Signal. 10 (2008) 739–753.
[10] J.D. Lang, P.J. McArdle, P.J. O'Reilly, S. Matalon, Oxidant-antioxidant balance in acute lung injury, Chest 122 (2002) 314s–320s.
[11] R. Ruffmann, Reactive oxygen species in acute lung injury, Eur. Respir. J. 12 (1998), 1486.
[12] R.F. Guo, P.A. Ward, Role of oxidants in lung injury during sepsis, Antioxidants Redox Signal. 9 (2007) 1991–2002.
[13] P.G. Metnitz, C. Bartens, M. Fischer, P. Fridrich, H. Steltzer, W. Druml, Antioxidant status in patients with acute respiratory distress syndrome, Intensive Care Med. 25 (1999) 180–185.
[14] H. Cai, K.K. Griendling, D.G. Harrison, The vascular NAD(P)H oxidases as therapeutic targets in cardiovascular diseases, Trends Pharmacol. Sci. 24 (2003) 471–478.
[15] Y. Zhang, P. Murugesan, K. Huang, H. Cai, NADPH oxidases and oxidase crosstalk in cardiovascular diseases: novel therapeutic targets, Nat. Rev. Cardiol. 17 (2020) 170–194.
[16] R.M. Touyz, A. Anagnostopoulou, F. Rios, A.C. Montezano, L.L. Camargo, NOX5: molecular biology and pathophysiology, Exp. Physiol. 104 (2019) 605–616.
[17] R.P. Brandes, N. Weissmann, K. Schroder, Nox family NADPH oxidases: molecular mechanisms of activation, Free Radic. Biol. Med. 76 (2014) 208–226.
[18] J.Y. Youn, L. Gao, H. Cai, The p47phox- and NADPH oxidase organiser 1 (NOXO1)-dependent activation of NADPH oxidase 1 (NOX1) mediates endothelial nitric oxide synthase (eNOS) uncoupling and endothelial dysfunction in a streptozotocin-induced murine model of diabetes, Diabetologia 55 (2012) 2069–2079.
[19] K. Bedard, K.H. Krause, The NOX family of ROS-generating NADPH oxidases: physiology and pathophysiology, Physiol. Rev. 87 (2007) 245–313.
[20] R.J. Colbran, Targeting of calcium/calmodulin-dependent protein kinase II, Biochem. J. 378 (2004) 1–16.
[21] H. Cai, D. Liu, J.G. Garcia, CaM Kinase II-dependent pathophysiological signalling in endothelial cells, Cardiovasc. Res. 77 (2008) 30–34.
[22] H. Cai, Hydrogen peroxide regulation of endothelial function: origins, mechanisms, and consequences, Cardiovasc. Res. 68 (2005) 26–36.
[23] J. Palomeque, O.V. Rueda, L. Sapia, C.A. Valverde, M. Salas, M.V. Petroff, A. Mattiazzi, Angiotensin II-induced oxidative stress resets the Ca^{2+} dependence of Ca^{2+}-calmodulin protein kinase II and promotes a death pathway conserved across different species, Circ. Res. 105 (2009) 1204–1212.
[24] A. Nguyen, P. Chen, H. Cai, Role of CaMKII in hydrogen peroxide activation of ERK1/2, p38 MAPK, HSP27 and actin reorganization in endothelial cells, FEBS Lett. 572 (2004) 307–313.
[25] Y. Xiong, C. Wang, L. Shi, L. Wang, Z. Zhou, D. Chen, J. Wang, H. Guo, Myosin light chain kinase: a potential target for treatment of inflammatory diseases, Front. Pharmacol. 8 (2017) 292.
[26] W.Q. He, J. Wang, J.Y. Sheng, J.M. Zha, W.V. Graham, J.R. Turner, Contributions of myosin light chain kinase to regulation of epithelial paracellular permeability and mucosal homeostasis, Int. J. Mol. Sci. 21 (2020).
[27] X. Cong, W. Kong, Endothelial tight junctions and their regulatory signaling pathways in vascular homeostasis and disease, Cell. Signal. 66 (2020), 109485.
[28] H. Chiba, M. Osanai, M. Murata, T. Kojima, N. Sawada, Transmembrane proteins of tight junctions, Biochim. Biophys. Acta 1778 (2008) 588–600.
[29] C. Zihni, C. Mills, K. Matter, M.S. Balda, Tight junctions: from simple barriers to multifunctional molecular gates, Nature reviews, Mole. Cell Biol. 17 (2016) 564–580.
[30] G. Bazzoni, E. Dejana, Endothelial cell-to-cell junctions: molecular organization and role in vascular homeostasis, Physiol. Rev. 84 (2004) 869–901.
[31] J.M. Bland, D.G. Altman, Survival probabilities (the Kaplan-Meier method), BMJ (Clin. Res. Ed.) 317 (1998), 1572.
[32] K.J. Jager, P.C. van Dijk, C. Zoccali, F.W. Dekker, The analysis of survival data: the Kaplan-Meier method, Kidney Int. 74 (2008) 560–565.
[33] S. Palumbo, Y.J. Shin, K. Ahmad, A.A. Desai, H. Quijada, M. Mohamed, A. Knox, S. Sammani, B.A. Colson, T. Wang, J.G. Garcia, L. Hecker, Dysregulated Nox4 ubiquitination contributes to redox imbalance and age-related severity of acute lung injury, Am. J. Physiol. Lung Cell Mol. Physiol. 312 (2017) L297–l308.
[34] K.T. Cheng, S. Xiong, Z. Ye, Z. Hong, A. Di, K.M. Tsang, X. Gao, S. An, M. Mittal, S. M. Vogel, E.A. Miao, J. Rehman, A.B. Malik, Caspase-11-mediated endothelial pyroptosis underlies endotoxemia-induced lung injury, J. Clin. Invest. 127 (2017) 4124–4135.
[35] R. Szulcek, H.J. Bogaard, G.P. van Nieuw Amerongen, Electric cell-substrate impedance sensing for the quantification of endothelial proliferation, barrier function, and motility, J. Visualized Exp. JoVE (85) (2014 Mar 28) 51300.
[36] K.L. Siu, L. Gao, H. Cai, Differential roles of protein complexes NOX1-NOXO1 and NOX2-p47phox in mediating endothelial redox responses to oscillatory and unidirectional laminar shear stress, J. Biol. Chem. 291 (2016) 8653–8662.
[37] J.H. Oak, H. Cai, Attenuation of angiotensin II signaling recouples eNOS and inhibits nonendothelial NOX activity in diabetic mice, Diabetes 56 (2007) 118–126.
[38] K.L. Siu, C. Lotz, P. Ping, H. Cai, Netrin-1 abrogates ischemia/reperfusion-induced cardiac mitochondrial dysfunction via nitric oxide-dependent attenuation of NOX4 activation and recoupling of NOS, J. Mol. Cell. Cardiol. 78 (2015) 174–185.
[39] H.D. Wang, S. Xu, D.G. Johns, Y. Du, M.T. Quinn, A.J. Cayatte, R.A. Cohen, Role of NADPH oxidase in the vascular hypertrophic and oxidative stress response to angiotensin II in mice, Circ. Res. 88 (2001) 947–953.
[40] K. Matsuno, H. Yamada, K. Iwata, D. Jin, M. Katsuyama, M. Matsuki, S. Takai, K. Yamanishi, M. Miyazaki, H. Matsubara, C. Yabe-Nishimura, Nox1 is involved in angiotensin II-mediated hypertension: a study in Nox1-deficient mice, Circulation 112 (2005) 2677–2685.
[41] M.A. Koay, J.W. Christman, B.H. Segal, A. Venkatakrishnan, T.R. Blackwell, S. M. Holland, T.S. Blackwell, Impaired pulmonary NF-kappaB activation in response to lipopolysaccharide in NADPH oxidase-deficient mice, Infect. Immun. 69 (2001) 5991–5996.
[42] H. Yao, I. Edirisinghe, S.R. Yang, S. Rajendrasozhan, A. Kode, S. Caito, D. Adenuga, I. Rahman, Genetic ablation of NADPH oxidase enhances susceptibility to cigarette smoke-induced lung inflammation and emphysema in mice, Am. J. Pathol. 172 (2008) 1222–1237.
[43] S.M. Dudek, E.T. Chiang, S.M. Camp, Y. Guo, J. Zhao, M.E. Brown, P.A. Singleton, L. Wang, A. Desai, F.T. Arce, R. Lal, J.E. Van Eyk, S.Z. Imam, J.G. Garcia, Abl tyrosine kinase phosphorylates nonmuscle Myosin light chain kinase to regulate endothelial barrier function, Mol. Biol. Cell 21 (2010) 4042–4056.
[44] T. Mirzapoiazova, J. Moitra, L. Moreno-Vinasco, S. Sammani, J.R. Turner, E. T. Chiang, C. Evenoski, T. Wang, P.A. Singleton, Y. Huang, Y.A. Lussier, D. M. Watterson, S.M. Dudek, J.G. Garcia, Non-muscle myosin light chain kinase isoform is a viable molecular target in acute inflammatory lung injury, Am. J. Respir. Cell Mol. Biol. 44 (2011) 40–52.
[45] P.V. Usatyuk, P.A. Singleton, S. Pendyala, S.K. Kalari, D. He, I.A. Gorshkova, S. M. Camp, J. Moitra, S.M. Dudek, J.G. Garcia, V. Natarajan, Novel role for non-muscle myosin light chain kinase (MLCK) in hyperoxia-induced recruitment of cytoskeletal proteins, NADPH oxidase activation, and reactive oxygen species generation in lung endothelium, J. Biol. Chem. 287 (2012) 9360–9375.
[46] T. Wang, M.E. Brown, G.T. Kelly, S.M. Camp, J.B. Mascarenhas, X. Sun, S. M. Dudek, J.G.N. Garcia, Myosin light chain kinase (MYLK) coding polymorphisms modulate human lung endothelial cell barrier responses via altered tyrosine phosphorylation, spatial localization, and lamellipodial protrusions, Pulm. Circ. 8 (2018), 2045894018764171.
[47] A. Hartsock, W.J. Nelson, Adherens and tight junctions: structure, function and connections to the actin cytoskeleton, Biochim. Biophys. Acta 1778 (2008) 660–669.
[48] E.E. Schneeberger, R.D. Lynch, Structure, function, and regulation of cellular tight junctions, Am. J. Physiol. 262 (1992) L647–L661.
[49] R. Shiomi, K. Shigetomi, T. Inai, M. Sakai, J. Ikenouchi, CaMKII regulates the strength of the epithelial barrier, Sci. Rep. 5 (2015), 13262.